Received: 18 November 2019 | Revised: 16 January 2020 | Accepted: 11 February 2020

DOI: 10.1002/pip.3258

RESEARCH ARTICLE

PROGRESS IN PHOTOVOLTAICS WILEY

Wide angle antireflection in metal nanoparticles embedded in a dielectric matrix for plasmonic solar cells

Bhaskar Singh[1] | Mohammed M. Shabat[2] | Daniel M. Schaadt[1]

[1]Institute of Energy Research and Physical Technologies, Clausthal University of Technology, Leibnizstraße 4, 38678, Clausthal-Zellerfeld, Germany

[2]Physics Department, Islamic University of Gaza, PO Box 108, Gaza Strip, Palestinian Authority

Correspondence
Bhaskar Singh, Institute of Energy Research and Physical Technologies, Clausthal University of Technology, Leibnizstraße 4, 38678 Clausthal-Zellerfeld, Germany.
Email: bhaskar.singh@tu-clausthal.de

Funding information
Bundesministerium für Bildung und Forschung, Grant/Award Number: NANOWAVSL:01DH17016

Abstract

The photon density in solar cells is usually optimized through tailored antireflection coatings (ARCs). We develop an analytical model to describe metal hybrid nanoparticles (NPs)-based ARC, where metal NPs are embedded in a standard ARC on a Si-substrate. A point dipole approach is implemented to calculate diffuse reflectance by NPs, while transfer matrix method is used for specular reflectance from front surface. We found that embedding metal NPs in SiN ARC enhances the antireflection property of the former at non-normal angles of incidence (AOI) of light. Electric field distribution patterns of radiation in the substrate by NPs are calculated for various AOI, which support the improvements in the antireflection property. Weighted solar power transmittances from ARCs are calculated, which show that Ag-NPs (radius = 35 nm) embedded in SiN (thickness = 70 nm) performs better than SiN for AOI over 74°, whereas Al-NPs (radius = 35 nm) embedded in SiN (thickness = 70 nm) performs better for AOI over 78°.

KEYWORDS

antireflection coating, metal nanoparticles, plasmonics, silicon, solar cells, transfer matrix method

1 | INTRODUCTION

Solar cells suffer loss from front surface reflection of incident sunlight. To reduce this loss, an antireflection coating (ARC) is typically used.[1-9] As an alternative, metal nanoparticles (NPs), which show plasmonic effect and scatter the sunlight efficiently at resonance wavelength, have been suggested.[10-15] The scattering and absorption properties of such NPs have been studied and modeled extensively in previous years.[16-23] Gold NPs (Au-NPs) at front side of Si solar cells[10] and silver NPs (Ag-NPs) at front side of GaAs solar cells[11] have been demonstrated with improved performance in efficiency of the solar cell device. In this configuration, metal NP layers act as an ARC. Lesina et al have modeled and characterized ARCs based on Ag-NPs embedded in a SiO_2 dielectric matrix on silicon solar cells.[24] They used finite-difference time-domain (FDTD) simulation and have stated that Ag-NPs within SiO_2 gives promising results, although the broadband performance of SiO_2-based ARC remains unbeaten at normal incidence. They also suggested that to complete the analysis, other metal NPs such as Al, Cu, and another ARC material such as SiN should be explored with thin-film solar cells. Thus far, most studies have been performed only for normal incidence, since commercially available solar cells are usually coated with an ARC, which is such that the reflectance is minimal for a wavelength near the maximum of the solar spectrum under normal incidence. But in reality, a fixed solar cell on a house roof receives the sunlight throughout the day at various angles of incidence (AOI) of a wide range of wavelengths. Thus, it is important to compare the performance of standard (pure dielectric-based ARC) and hybrid ARC (NPs embedded in the dielectric-based ARC) at various AOI.

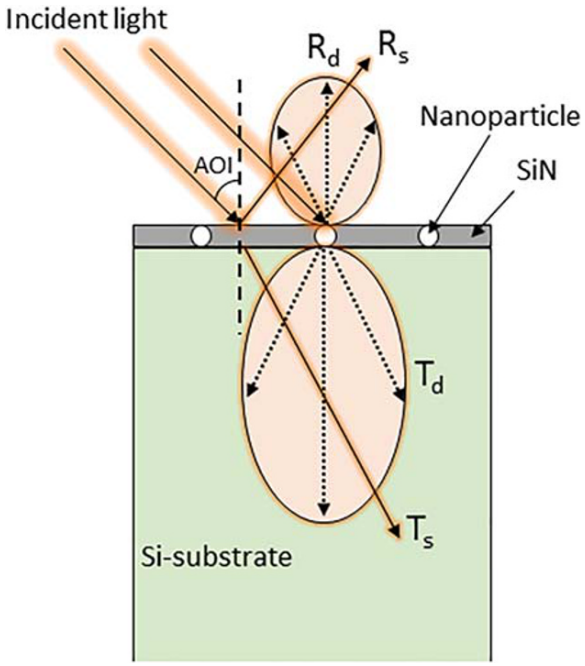

FIGURE 1 Schematic of the simulated device structure [Colour figure can be viewed at wileyonlinelibrary.com]

In this paper, we present an analytical model that combines transfer matrix method (TMM)[25,26] with Mie theory[27,28] to model the optical properties of NPs-based ARCs on a Si-substrate. When the sunlight incident on a rough interface (the hybrid ARC layer in our case), reflectance from interface divides into two parts—specular reflectance (R_s) and diffuse reflectance (R_d), similarly for transmittance as shown in Figure 1.[29] The specularly reflected light is obtained by efficient TMM method of multilayer structures, whereas for the diffusely reflected light, angular power distribution of radiation by an NP in the substrate is calculated.[30] It is assumed in the current study that the specular and diffuse reflectance occurrences are independent of each other and do not interfere.

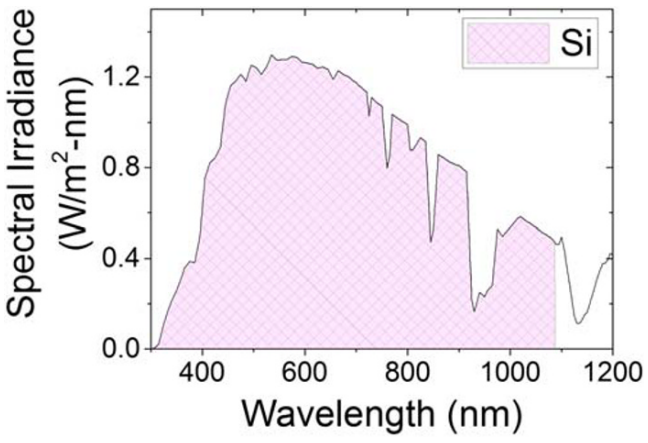

FIGURE 2 AM1.5D solar spectrum. Only shaded area is available for a Si absorber [Colour figure can be viewed at wileyonlinelibrary.com]

2 | DEVICE STRUCTURE AND THEORY

A hybrid ARC made of nanocomposite (NPs and host medium), in which NPs are in a two-dimensional (2-D) array of equal period in a dielectric SiN matrix bounded with air and the substrate, is investigated. A schematic of the simulated device structure is shown in

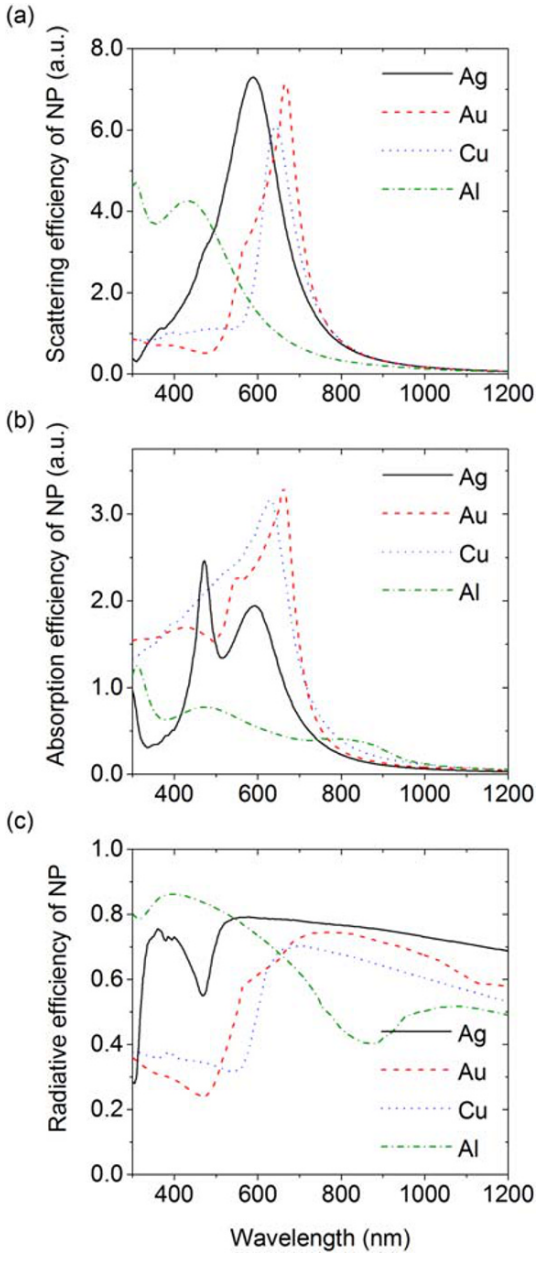

FIGURE 3 (a) Scattering, (b) absorption, and (c) radiative efficiencies of nanoparticles (NP) (radius = 35 nm) versus the light operating wavelength [Colour figure can be viewed at wileyonlinelibrary.com]

Figure 1. The optical properties of NPs have been calculated in terms of dimensionless quantities such as scattering efficiency (Q_{sca}) and absorption efficiency (Q_{abs}). The sum of both efficiencies is called extinction efficiency (Q_{ext}) of NPs. Radiative efficiency (Q_{rad}) of NPs equals to Q_{sca}/Q_{ext}, which tells how much light get scattered from and absorbed in the NP.

The TMM, also called 2 × 2 matrix method, is generally applied to determine reflection, transmission, and absorption in a multilayer thin film.[25,26] A plane wave incident on the proposed device is assumed. The SiN layer has a thickness of d_1 with refractive index n_1. Therefore, a transmission matrix for the SiN layer can be written as

$$M_{jk} = \frac{1}{t_{jk}}\begin{bmatrix} 1 & r_{jk} \\ r_{jk} & 1 \end{bmatrix}, \quad (1)$$

where t_{jk} and r_{jk} are the Fresnel transmission and reflection coefficients at an interface jk. A propagation matrix for the wave propagating through the SiN layer is given by

$$P_1 = \begin{bmatrix} e^{-i.(2\pi/\lambda).d_1.n_1.\cos(\theta_1)} & 0 \\ 0 & e^{i.(2\pi/\lambda).d_1.n_1.\cos(\theta_1)} \end{bmatrix}, \quad (2)$$

where λ and θ_1 are wavelength of the incident wave and angle of refraction in the SiN layer, respectively. By using the transmission matrix and the propagation matrix, the total transfer matrix, $\boldsymbol{M}$, for the device is given by

$$\boldsymbol{M} = M_{01}.P_1.M_{1s} = \begin{bmatrix} \boldsymbol{M_{11}} & \boldsymbol{M_{12}} \\ \boldsymbol{M_{21}} & \boldsymbol{M_{22}} \end{bmatrix}. \quad (3)$$

The transmission and reflection coefficients can be expressed from Equation (3) as $t = \frac{1}{M_{11}}; r = \frac{M_{21}}{M_{11}}$.

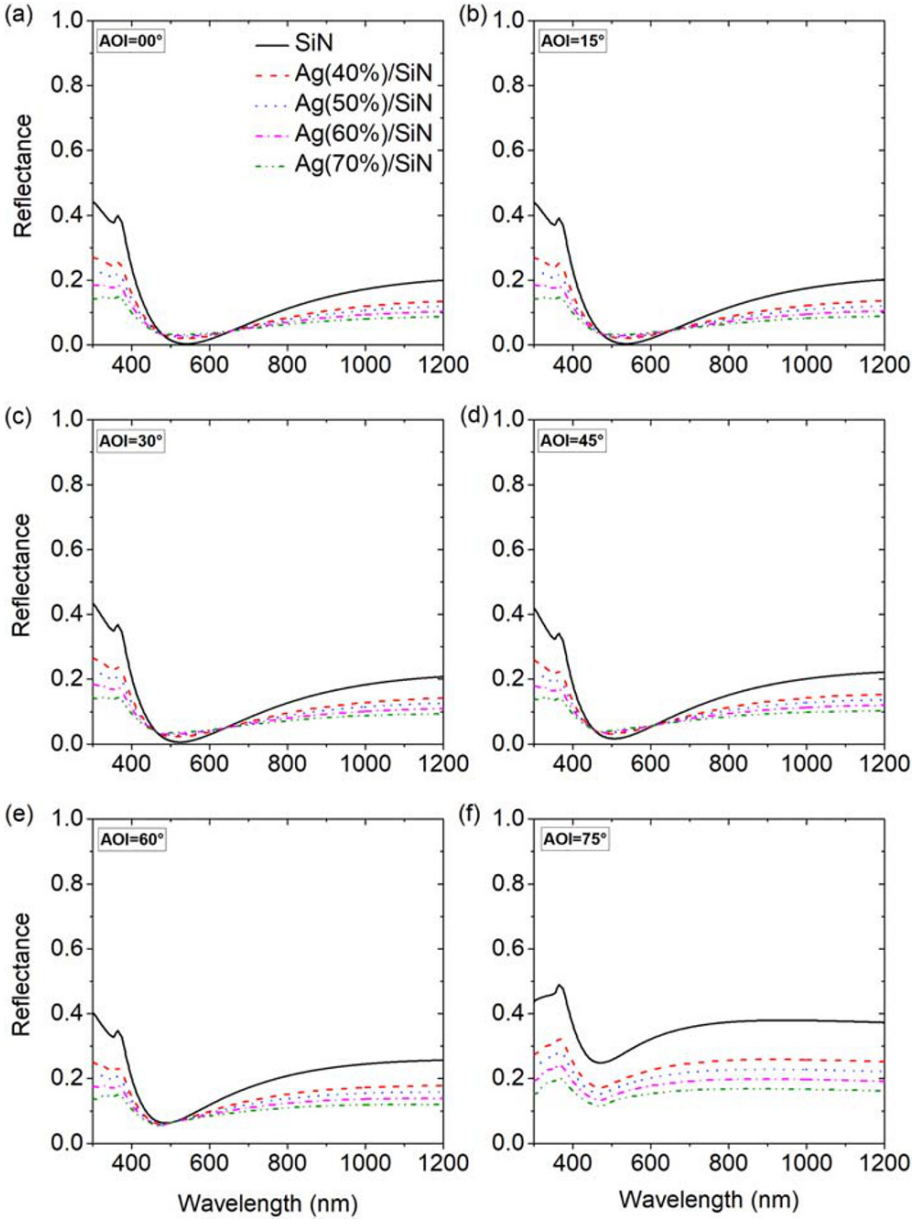

FIGURE 4 Reflectance from Ag-NPs/SiN layer versus the light operating wavelength. Bottom layer is Si-substrate as shown in Figure 1. AOI = 00° corresponds to normal incidence. Ag(40%)/SiN refers that 40% surface cross section is covered by Ag-NPs and the rest is SiN. AOI, angle of incidence; NPs, nanoparticles [Colour figure can be viewed at wileyonlinelibrary.com]

From above results, the specular reflectance is expressed as $\boldsymbol{R_s} = |r|^2$ and the specular transmittance is expressed as $\boldsymbol{T_s} = \frac{n_s \cos(\theta_s)}{n_0 \cos(\theta_0)} \cdot |t|^2$, where s and 0 are corresponding to the substrate and incident medium (air).

Mie[27, 28] obtained a solution for the interaction of a plane electromagnetic wave by homogeneous spheres of arbitrary index of refraction embedded in a homogeneous dielectric medium. The solutions are expressed in infinite series as extinction (Q_{ext}) and scattering efficiency (Q_{sca}) of a homogeneous sphere:

$$Q_{ext} = \frac{2}{x^2}\sum_{n=1}^{\infty}(2n+1)\,Re[a_n + b_n],\; Q_{sca} = \frac{2}{x^2}\sum_{n=1}^{\infty}(2n+1)\left[(a_n)^2 + (b_n)^2\right], \tag{4}$$

where $a_n = \frac{m\psi_n(mx)\psi'_n(x) - \psi_n(x)\psi'_n(mx)}{m\psi_n(mx)\xi'_n(x) - \xi_n(x)\psi'_n(mx)}$, $b_n = \frac{\psi_n(mx)\psi'_n(x) - m\psi_n(x)\psi'_n(mx)}{\psi_n(mx)\xi'_n(x) - m\xi_n(x)\psi'_n(mx)}$, and size parameter x is $2\pi n_1 r/\lambda$. m is ratio of refractive index of NP (n_r) to that of surrounding medium (n_1); ψ_n and ξ_n are Riccati-Bessel functions; and r is radius of the sphere.

In a dipole model, the NP is assumed as a dipole oscillating at its resonant frequency. The dipole generally excites in the direction of polarization of the incident light (regardless of front and back illumination). Therefore, the excitation angle changes with the AOI of light. Mertz[30] has formulated a dipole radiating at a distance near a substrate and found an expression for the angular power distribution of scattered light from the NP in air and in the neighboring substrate, which is as follows:

$$L_\phi(\theta) = L^{s,p}(\theta)\sin^2(\phi) + L^p_\perp(\theta)\cos^2(\phi) + Re\left[L^p_X(\theta)\right]\sin 2\phi, \tag{5}$$

where θ is the observation angle and ϕ is the inclination of the dipole from vertical. The derivation of Equation (5) and explanations of $L^{s,p}$, $L^p_\perp$, and L^p_X can be found in Mertz.[30]

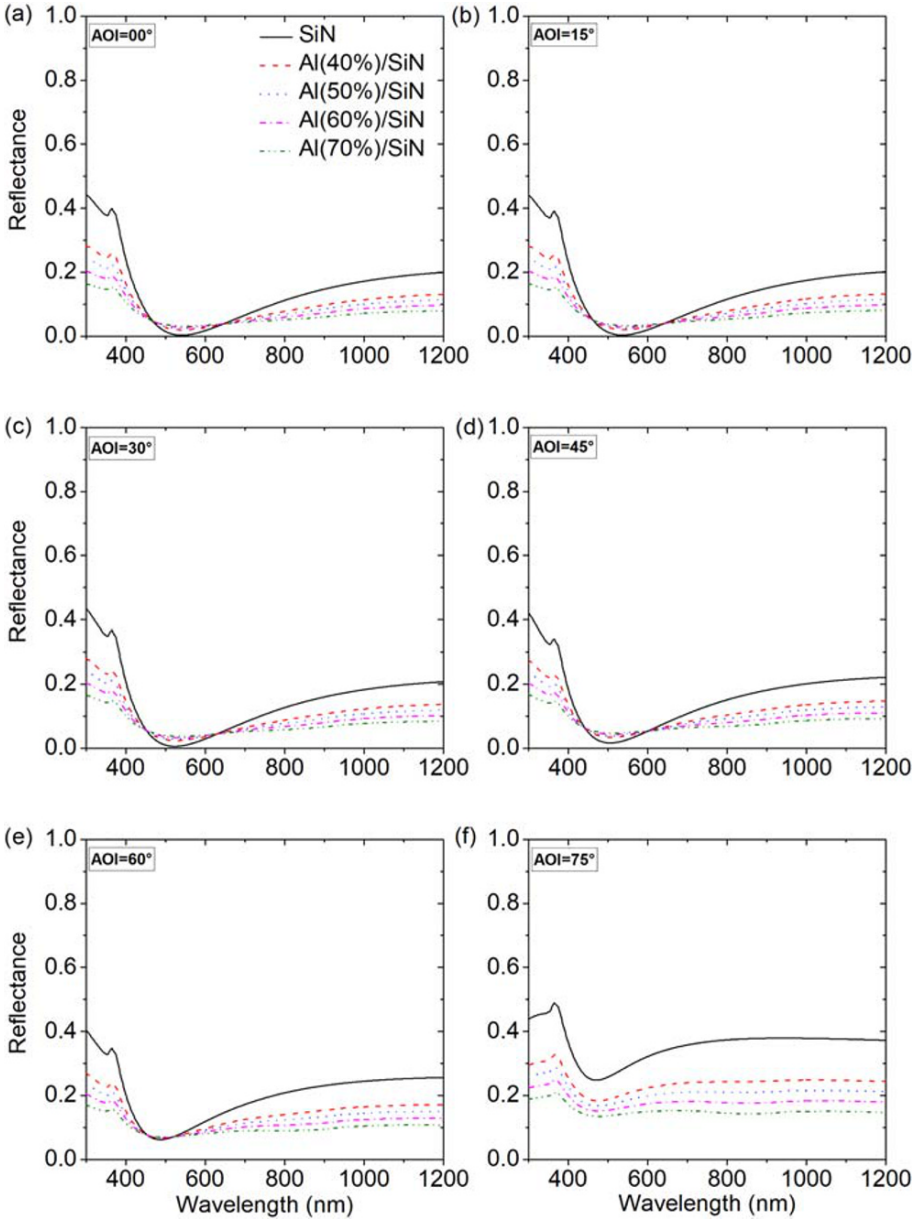

FIGURE 5 Reflectance from Al-NPs/SiN layer versus the light operating wavelength. Bottom layer is Si-substrate as shown in Figure 1. AOI = 00° corresponds to normal incidence. Al(40%)/SiN refers that 40% surface cross section is covered by Al-NPs and the rest is SiN. AOI, angle of incidence; NPs, nanoparticles [Colour figure can be viewed at wileyonlinelibrary.com]

The diffused reflectance and transmittance can be given from above equations as

$$\boldsymbol{R_d} = Q_{sca} * \frac{1}{\pi}\int_0^{\pi} L_{\phi}(\theta)(\text{reflected})\, d\theta \text{ and } \boldsymbol{T_d} = Q_{sca} * \frac{1}{\pi}\int_0^{\pi} L_{\phi}(\theta)(\text{transmitted})\, d\theta. \tag{6}$$

The sum of both reflectance (specular and diffuse) is the total reflectance from the front surface of device such as

$$\boldsymbol{R} = f * \boldsymbol{R_d} + (1-f) * \boldsymbol{R_s}, \tag{7}$$

where f is fraction of cross section area covered by NPs at the front surface. The dipole approximation is valid when distance between the NPs are of the order of or more than their diameters such that $f < 0.75$.

Optical constants of metal NPs and refractive indices of SiN for the calculations are taken from Palik.[31] Linear interpolation is used to fit the optical constants to desired step size. The solar spectrum used in calculation is taken from Buie et al[7] and is shown in Figure 2. An angular dependent solar spectrum is ignored as it has no effect on reflectance calculation. The study has been done on four different NP densities in the nanocomposite. The nomenclature of the nanocomposite layer: Ag(40%)/SiN refers that 40% surface cross section is covered by Ag-NPs and the rest is SiN. In the simulations, the SiN layer thickness is kept at 70 nm and NP radius at 35 nm.

3 | SIMULATION RESULTS

Figure 3 shows the scattering, absorption, and radiation efficiencies of NP. Ag- and Au-NP show strong dipole resonance scattering peak in visible range at 589 and 666 nm, respectively. Cu-NP have lower peak than Ag- and Au-NP in the same range at 643 nm. A higher order resonance mode is visible in the absorption of Ag-NP at 472 nm. Al-NP has a relatively weak resonance peak. Localized surface plasmon resonance in metals is predominantly due to behavior of free electrons in conduction band, whereas interband transitions damp or prohibit this transition. The noble metals (Ag, Au, and Cu) are distinguished by a threshold below which the optical properties of metals are dominated

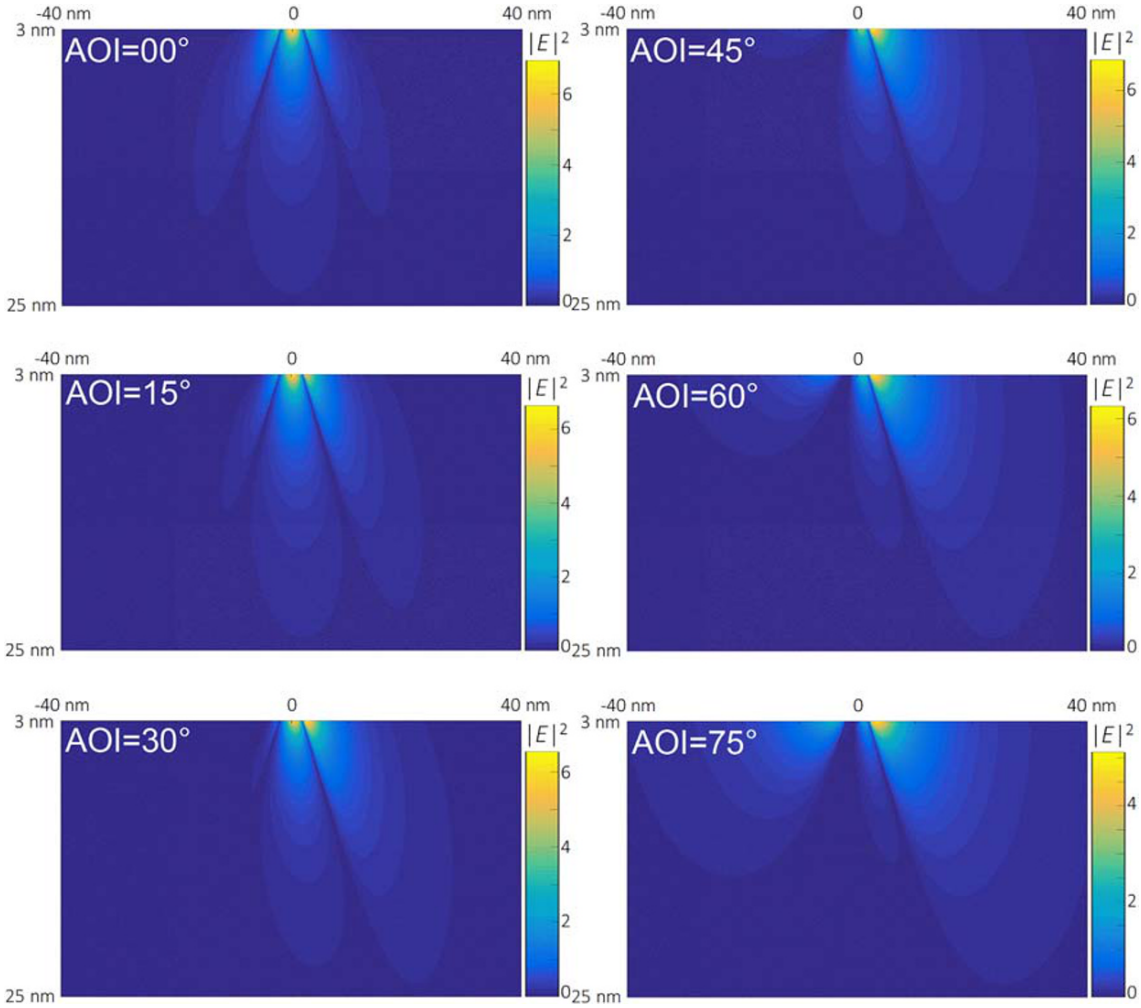

FIGURE 6 Electric field distribution patterns of light (λ = 510 nm) radiated from Ag-NP (radius = 35 nm) in Si substrate. AOI = 00° corresponds to normal incidence. AOI, angle of incidence; NPs, nanoparticles [Colour figure can be viewed at wileyonlinelibrary.com]

by the interband transition. This transition occurs at wavelengths 468, 477, and 539 nm for Ag-, Au-, and Cu-NP, respectively, in our case (Figure 3c). Al has a weak interband region near 875 nm.[16] The most useful quantity of NP for the ARC application is Q_{rad}. The Q_{rad} graph shows that Ag-NP has high radiation at 575 nm where the solar spectrum is at maximum. Al-NP also follows the solar spectrum graph. This makes them promising to incorporate in conventional SiN ARC.

Figure 4 shows the reflectance spectra of the simulated device structure with Ag-NPs in SiN at various AOI. At normal incidence (AOI = 00°), SiN shows the best performance. The reflectance minimum in this case is obtained at 536 nm. Ag(70%)/SiN shows the worst performance at normal incidence and reflects 10% to 20% of the incident light on average from the entire solar spectrum. As AOI of the light changes from normal to non-normal angle, we obtained increase in the reflection of SiN ARC. At 60° AOI, the reflectance curves of SiN ARC and NPs-based ARC become almost equal. And after this, NPs-based ARC outperform SiN ARC. Ag(70%)/SiN shows better performance among all the ARCs at higher AOI. SiN ARC shows around 40% reflection at 75° AOI. When SiN ARC reaches near to its critical angle at higher AOI, the reflectance becomes higher, whereas NPs do not show this behavior and performs better at higher AOI. Al-NPs also exhibits improvement in ARC performance at higher AOI. Figure 5 shows the reflectance spectra of the simulated device structure with Al-NPs at various AOI. The difference in reflectance between Ag-NPs and Al-NPs can be seen only at higher AOI, where the reflectance curves of NPs-based ARC shows the same behavior as the radiative efficiency curves of NP.

The electric field distribution profile of the light radiated from Ag-NP in the substrate is shown in Figure 6. At higher AOI, the Ag-NP radiates with the same order of intensity as at normal incidence, which is the reason that the NPs-based ARC performs

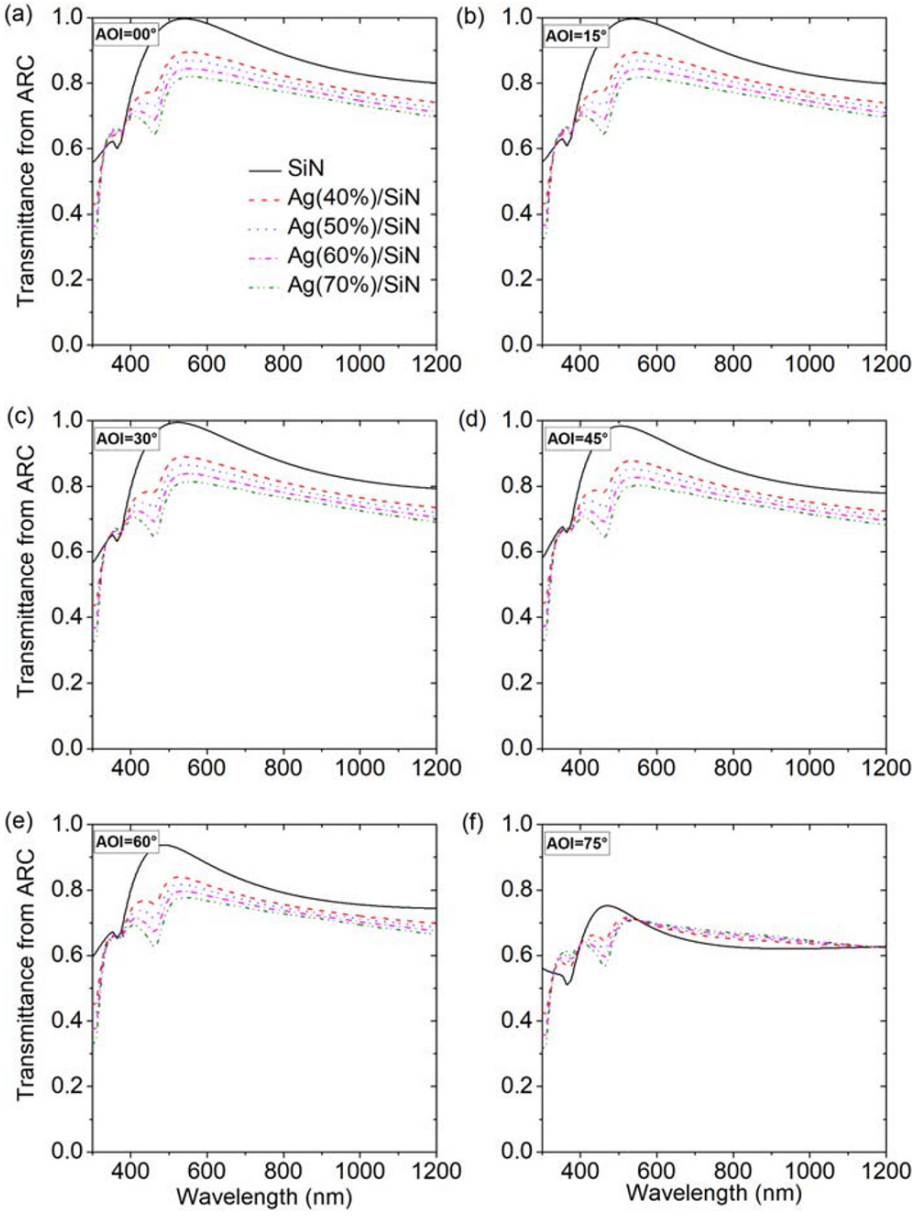

FIGURE 7 Transmittance from Ag-NPs/SiN layer into Si-substrate versus the light operating wavelength. AOI = 00° corresponds to normal incidence. Ag(40%)/SiN refers that 40% surface cross section is covered by Ag-NPs and the rest is SiN. AOI, angle of incidence; NPs, nanoparticles [Colour figure can be viewed at wileyonlinelibrary.com]

relatively better than SiN ARC at higher AOI. The figure at normal incidence looks same as reported in Schmid et al.[22] The angular distribution of radiation in the substrate also benefits in waveguide-based trapping of the incident light. Soller and Hall reported that more than 80% of light radiated from dipole directs into the waveguide mode.[32] And Catchpole and Pillai measured experimentally enhancement in absorption by a factor of 7.5 due to the waveguide mode coupling.[33]

The ARCs in solar cells are designed to minimize the reflectance and maximize the transmittance across the wavelength range of interest. Since the transmittance needs to be maximized where the solar spectrum has maximum intensity, we have calculated weighted solar power transmittance (T_w):

$$T_w = \frac{\int_{\lambda_1}^{\lambda_2} T(\lambda)\, S(\lambda)\, d\lambda}{\int_{\lambda_1}^{\lambda_2} S(\lambda)\, d\lambda}, \tag{8}$$

where $T(\lambda)$ and $S(\lambda)$ are the transmittance and intensity of the AM1.5D solar spectrum at wavelength λ. λ_1 and λ_2 are the minimum and maximum allowed wavelengths.

Figure 9 shows the T_w curves of SiN ARC and metal NPs-based ARC. SiN ARC shows more than 90% transmittance at normal incidence as expected (Figure 9a,b). At 74° AOI, Ag-NPs/SiN and SiN have equal values. After 74° AOI, Ag-NPs–based ARC shows better performance than SiN ARC. In Al-NPs–based ARC, this happens at around 78° AOI. Therefore, 74° AOI plays a barrier for Ag-NPs–based ARC and 78° AOI for Al-NPs–based ARC. Before this barrier, SiN ARC performs better, and after this barrier, NPs-based ARC performs better. Between Ag-NPs and Al-NPs, Ag-NPs performs better than Al-NPs at any AOI. The reflectance curves of Ag-NPs/SiN (Figure 4) and of Al-NPs/SiN (Figure 5) show better performance than SiN, but in transmittance curves, they show opposite behavior as shown in Figures 7 and 8. This is because of the parasitic absorption in NPs,

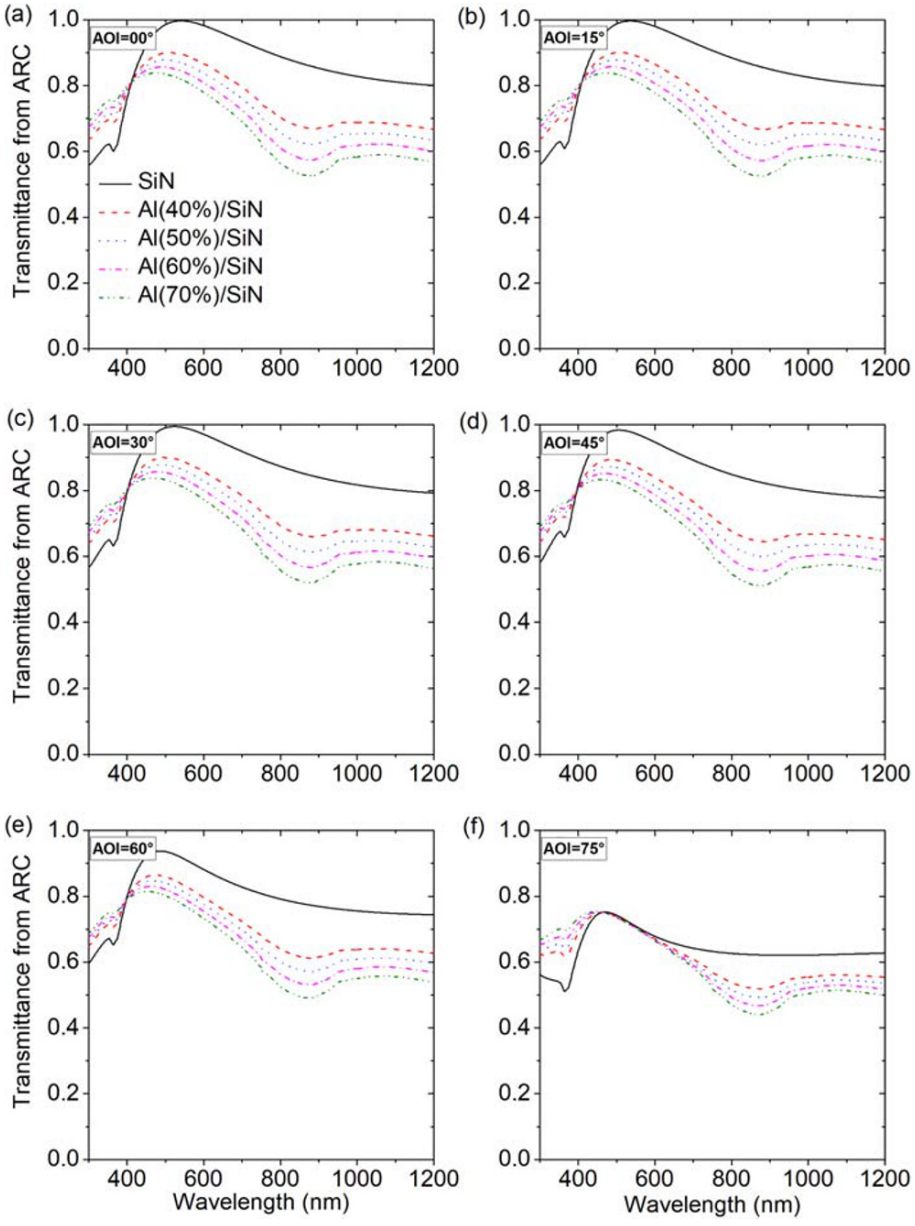

FIGURE 8 Transmittance from Al-NPs/SiN layer into Si-substrate versus the light operating wavelength. AOI = 00° corresponds to normal incidence. Al(40%)/SiN refers that 40% surface cross section is covered by Al-NPs and the rest is SiN. AOI, angle of incidence; NPs, nanoparticles [Colour figure can be viewed at wileyonlinelibrary.com]

when in fact there is almost no absorption in SiN. This emphasizes the use of metal NPs with less parasitic absorption as an ARC. The NPs with high scattering and absorption properties are good to use as a rear side reflector.[34-36] SiN(45) and SiN(75) curves in Figure 9a are optimized for T_w at AOI = 45° and AOI = 75°, respectively.

4 | DISCUSSION

The scattering and absorption in the NPs are highly influenced by the size and host medium of the NPs. The geometric cross section of a metal NP is generally smaller than the optical cross section, which means that smaller NPs absorb more than bigger ones.[37] On the other hand, the solar cell absorber layers have different absorption range. Therefore, optimization of metal NPs with a solar cell absorber is the primary task to reduce the absorption loss in NPs. Ag-NPs have small absorption in the visible range, but it shows maximum radiation near the maxima of solar spectrum. Al-NPs have absorption range in near-infrared region, although Au- and Cu-NPs have poor radiative efficiency in the visible range (Figure 3c). Considering these factors,

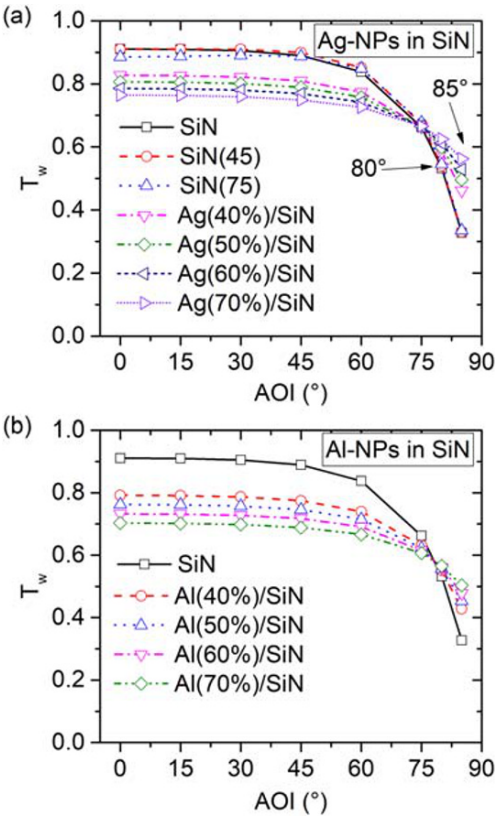

FIGURE 9 Weighted solar power transmittance (T_w) (a) from Ag-NPs/SiN layer, and (b) from Al-NPs/SiN into Si substrate. AOI = 00° corresponds to normal incidence. Ag(40%)/SiN and Al(40%)/SiN refer that 40% surface cross section is covered by Ag-NPs and Al-NPs, respectively; and the rest is SiN. Curve SiN(45): T_w optimized for AOI = 45°. Curve SiN(75): T_w optimized for AOI = 75°. AOI, angle of incidence; NPs, nanoparticles [Colour figure can be viewed at wileyonlinelibrary.com]

Ag-NPs simply outperform on the choice of metal NPs for ARC application. The host medium also changes the optical properties of metal NPs by shifting the resonance wavelength, which is further a way to alleviate the parasitic absorption of desired wavelength in metal NPs.[16] In our study, we focused to SiN as a host medium to present our idea, albeit it is not limited.

In this study, we have restricted ourselves to spherical NPs for less complexity in NP structure and because these are easy to model analytically. However, the shape of NPs plays a major role in the scattering of sunlight to the neighboring substrate. Atwater and Polman have published a review article and have shown that the cylindrical shape of Ag-NP scatters more fraction of the incident sunlight in the substrate than the spherical one.[20] The fraction of radiation by a dipole also varies with the position of NPs. It radiates more fraction of light in the substrate when in contact with the substrate than when in air.[19] Therefore, NPs embedded in an ARC must be in contact with the substrate.

Our study can be used to guide future experimental design. The optimizations of experimental work such as the optimization of nanoparticles size, the optimization of nanostructures etc. might lead to even better performance than that predicted by the simulations.[20] In this study, we performed the analysis to calculate the antireflection property of metal NPs embedded in a SiN layer and weighted solar power transmittance from the ARC layers into the substrate under incidence of the AM1.5D solar spectrum. However, this model can be extended to the analysis of net power gain in a device from 1 day to a whole year for a specific location and orientation.

5 | CONCLUSIONS

We performed a theoretical study on metal NPs with a Si-substrate over a wide AOI of the AM1.5D solar spectrum. An analytical model was developed for the analysis of ARCs based on metal NPs embedded in a SiN dielectric matrix in a 2-D array on the surface of substrate. A point dipole approach with TMM method was implemented to calculate the total reflectance by NPs-based ARC. We found that metal NPs enhance the antireflection property of conventional SiN ARC at non-normal AOI. At normal incidence, SiN ARC still performs the best. Electric field distribution patterns of radiation by NPs in the substrate support the improvements in antireflection performance. We also obtained weighted solar power transmittance curves, which shows that Ag-NPs in SiN performs better than SiN over 74° AOI, whereas Al-NPs in SiN performs better over 78° AOI. Maximum surface covered by metal NPs have shown high power transmittance at higher AOI.

ACKNOWLEDGEMENT

The authors acknowledge Bundesministerium für Bildung und Forschung (BMBF) funding (NANOWAVSL:01DH17016). MMS acknowledges support of Alexander von Humboldt Foundation. BS thanks Sumeet Rohilla for valuable suggestions on simulation.

ORCID

Bhaskar Singh https://orcid.org/0000-0002-2998-9268

REFERENCES

1. Young PA, Thege WG. Two-layer laser anti-reflection coatings. *J Phys D Appl Phys*. 1971;4(1):64-71.
2. Bouhafs D, Moussi A, Chikouche A, Ruiz JM. Design and simulation of antireflection coating systems for optoelectronic devices: application to silicon solar cells. *Solar Energy Mater Solar Cells*. 1998;52(1-2):79-93.
3. Aziz WJ, Ramizy A, Ibrahim K, Hassan Z, Omar K. The effect of anti-reflection coating of porous silicon on solar cells efficiency. *Optik*. 2011;122:1462-1465.
4. Aiken DJ. High performance anti-reflection coatings for broadband multi junction solar cells. *Solar Energy Mater Solar Cells*. 2000;64:393-404.
5. Gangopadhyay U, Kim K, Mangalaraj D, Yi J. Low cost CBD ZnS anti-reflection coating on large area commercial mono-crystalline silicon solar cells. *Appl Surf Sci*. 2004;230:364-370.
6. Zhao J, Green MA. Optimized antireflection coatings for high efficiency silicon solar cells. *IEEE Trans Electr Devices*. 1991;38:1925-1934.
7. Buie D, McCann MJ, Weber KJ, Dey CJ. Full day simulations of anti-reflection coating for flat plate silicon photovoltaics. *Solar Energy Mater Solar Cells*. 2004;81:13-24.
8. Saylan S, Milakovich T, Hadi SA, Nayfeh A, Fitzgerald EA, Dahlem MS. Multilayer antireflection coating design for GaAs0.69P0.31/Si dual-junction solar cells. *Solar Energy*. 2015;122:76-86.
9. Boden SA, Bagnall DM. Sunrise to sunset optimization of thin film antireflective coatings for encapsulated, planer silicon solar cells. *Prog Photovoltaics: Res Appl*. 2009;17(4):241-252.
10. Schaadt DM, Feng B, Yu ET. Enhanced semiconductor optical absorption via surface plasmon excitation in metal nanoparticles. *Appl Phys Lett*. 2005;86(6):063106-1-063106-3.
11. Nakayama K, Tanabe K, Atwater HA. Plasmonic nanoparticle enhanced light absorption in GaAs solar cell. *Appl Phys Lett*. 2008;93(12):121904-1-121904-3.
12. Derkacs D, Lim SH, Matheu P, Mar W, Yu ET. Improved performance of amorphous silicon solar cells via scattering from surface plasmon polaritons in nearby metallic nanoparticles. *Appl Phys Lett*. 2006;89(9):093103-1-093103-3.
13. Hong L, Rusli, Wang X, et al. Design principles for plasmonic thin film GaAs solar cells with high absorption enhancement. *J Appl Phys*. 2012;112(5):054326-1-054326-5.
14. Ouyang Z, Zhao X, Varlamov S, Tao Y, Wong J, Pillai S. Nanoparticle-enhanced light trapping in thin-film silicon solar cells. *Prog Photovoltaics: Res Appl*. 2011;19:917-926.
15. Li X, Li PC, Hu DZ, Schaadt DM, Yu ET. Light trapping in thin-film solar cells via scattering by nanostructured antireflection coatings. *J Appl Phys*. 2013;114(4):044310-1-044310-7.
16. Temple TL, Bagnall DM. Broadband scattering of the solar spectrum by spherical metal nanoparticles. *Prog Photovoltaics: Res Appl*. 2013;21:600-611.
17. Cole JR, Halas NJ. Optimized plasmonic nanoparticle distributions for solar spectrum harvesting. *Appl Phys Lett*. 2006;89:153120-153122.
18. Kelly KL, Coronado EA, Zhao LL, Schatz GC. The optical properties of metal nanoparticles: the influence of size, shape, and dielectric environment. *J Phys Chem B*. 2003;107:668-677.
19. Catchpole KR, Polman A. Plasmonic solar cells. *Opt Express*. 2008;16(26):21793-21800.
20. Atwater HA, Polman A. Plasmonics for improved photovoltaic devices. *Nat Mater*. 2010;9(3):205-213.
21. Stuart HR, Hall DG. Island size effects in nanoparticle-enhanced photodetectors. *Appl Phys Lett*. 1998;73(26):3815-3817.
22. Schmid M, Klenk R, Lux-Steiner MC, Topic M, Krc J. Modeling plasmonic scattering combined with thin-film optics. *Nanotechnology*. 2011;22(2):025204 (10pp).
23. Kluczyk K, David C, Jacak J, Jacak W. On modeling of plasmon-induced enhancement of the efficiency of solar cells modified by metallic nano-particles. *Nanomaterials*. 2019;9:3 (28pp).
24. Lesina AC, Paternoster G, Mattedi F, et al. Modeling and characterization of antireflection coatings with embedded silver nanoparticles for silicon solar cells. *Plasmonics*. 2015;10(6):1525-1536.
25. Yeh P. *Optical Waves in Layered Media*. New York: Wiley & Sons; 1998.
26. Shabat MM, El-Amassi DM, Schaadt DM. Design and analysis of multilayer waveguides containing nanoparticles for solar cells. *Soalr Energy*. 2016;137:409-412.
27. Mie G. Beiträge zur Optik trüber Medien, speziell kolloidaler Metallösungen; von Gustav Mie. *Ann Phys*. 1908;4:377-445.
28. Bohren CF, Huffman DR. *Absorption and scattering of light by small particles*. New York: Wiley-Interscience; 1983:82-157.
29. Leblanc F, Perrin J, Schmitt J. Numerical modeling of the optical properties of hydrogenated amorphous silicon-based p-i-n solar cells deposited on rough transparent conducting oxide substrates. *J Appl Phys*. 1994;75(2):1074-1087.
30. Mertz J. Radiative absorption, fluorescence, and scattering of a classical dipole near a lossless interface: a unified description. *J Opt Soc Am B*. 2000;17(11):1906-1913.
31. Palik ED. *Handbook of Optical Constants of Solids*. New York: Academic; 1998.
32. Soller BJ, Hall DG. Energy transfer at optical frequencies to silicon-based waveguiding structures. *J Opt Soc Am A*. 2001;18(10):2577-2584.
33. Catchpole KR, Pillai S. Absorption enhancement due to scattering by dipoles into silicon waveguides. *J Appl Phys*. 2006;100(4):044504-1-044504-8.
34. Mendes MJ, Morawiec S, Simone F, Priolo F, Crupi I. Colloidal plasmonic back reflectors for light trapping in solar cells. *Nanoscale*. 2014;6(9):4796-4805.
35. Morawiec S, Mendes MJ, Mirabella S, Simone F, Priolo F, Crupi I. Self assembled silver nanoparticles for plasmon-enhanced solar cell back reflectors: correlation between structural and optical properties. *Nanotechnology*. 2013;24(26):265601 (11pp).
36. Tan H, Santbergen R, Yang G, Smets AHM, Zeman M. Combined optical and electrical design of plasmonic back reflector for high-efficiency thin-film silicon solar cells. *IEEE J Photovoltaics*. 2013;3(1):53-58.
37. Bohren CF. How can a particle absorb more than the light incident on it? *Am J Phys*. 1983;51(4):323-327.

How to cite this article: Singh B, Shabat MM, Schaadt DM. Wide angle antireflection in metal nanoparticles embedded in a dielectric matrix for plasmonic solar cells. *Prog Photovolt Res Appl*. 2020;28:682–690. https://doi.org/10.1002/pip.3258